Click Here for Full Article

Swash-aquifer interaction in the vicinity of the water table exit point on a sandy beach

Nick Cartwright,[1] Tom E. Baldock,[2] Peter Nielsen,[2] Dong-Sheng Jeng,[3] and Longbin Tao[1]

[1] The coupling of sandy beach aquifers with the swash zone in the vicinity of the water table exit point is investigated through simultaneous measurements of the instantaneous shoreline (swash front) location, pore pressures and the water table exit point. The field observations reveal new insights into swash-aquifer coupling not previously gleaned from measurements of pore pressure only. In particular, for the case where the exit point is seaward of the observation point, the pore pressure response is correlated with the distance between the exit point and the shoreline in that when the distance is large the rate of pressure drop is fast and when the distance is small the rate decreases. The observations expose limitations in a simple model describing exit point dynamics which is based only on the force balance on a particle of water at the sand surface and neglects subsurface pressures. A new modified form of the model is shown to significantly improve the model-data comparison through a parameterization of the effects of capillarity into the aquifer storage coefficient. The model enables sufficiently accurate predictions of the exit point to determine when the swash uprush propagates over a saturated or a partially saturated sand surface, potentially an important factor in the morphological evolution of the beach face. Observations of the shoreward propagation of the swash-induced pore pressure waves ahead of the runup limit shows that the magnitude of the pressure fluctuation decays exponentially and that there is a linear increase in time lags, behavior similar to that of tidally induced water table waves. The location of the exit point and the intermittency of wave runup events is also shown to be significant in terms of the shore-normal energy distribution. Seaward of the mean exit point location, peak energies are small because of the saturated sand surface within the seepage face acting as a "rigid lid" and limiting pressure fluctuations. Landward of the mean exit point the peak energies grow before decreasing landward of the maximum shoreline position.

1. Introduction

[2] Swash-aquifer interactions have been linked to the mobility of sediments on the beach face [e.g., *Turner and Nielsen*, 1997; *Elfrink and Baldock*, 2002] and hence to the dynamics of the intertidal zone. In particular, the location of the water table exit point on the beach has been shown to be an important factor in the morphological evolution of beaches [e.g., *Turner*, 1995].

[3] Time-averaging of the beach groundwater response to wave forcing reveals a localized seaward directed circulation cell [*Longuet-Higgins*, 1983; *Li and Barry*, 2000] which has implications for the availability and quality of coastal groundwater resources and for the fate of contaminants [e.g., *Li et al.*, 1999; *Moore*, 1999]. The dynamics of the water table exit point on the beach face have also been linked to the distribution of interstitial macrofauna [e.g., *McArdle and McLachlan*, 1991] and to aeolian sediment transport on beaches [e.g., *Jackson and Nordstrom*, 1997].

[4] Most previous investigations into the coupling of the ocean with coastal aquifers have been based on tidally induced water table fluctuations [e.g., *Lanyon et al.*, 1982; *Nielsen*, 1990; *Baird and Horn*, 1996; *Li et al.*, 1997a; *Baird et al.*, 1998; *Raubenheimer et al.*, 1999] although field observations from exposed coasts have shown that wave forcing is at least as important [e.g., *Kang et al.*, 1994; *Turner et al.*, 1997; *Nielsen*, 1999; *Cartwright et al.*, 2004a]. Until recently, the coupling of the swash zone with the porous beach matrix had received relatively little attention.

[5] In the early studies of *Waddell* [1976, 1980] and *Lewandowski and Zeidler* [1978] the analysis of their field observations focused on describing the nonlinear filtering effect of the porous matrix. The preferential damping of

---

[1]School of Engineering, Griffith University, Gold Coast, Queensland, Australia.
[2]Division of Civil Engineering, University of Queensland, Brisbane, Queensland, Australia.
[3]School of Civil Engineering, University of Sydney, Sydney, New South Wales, Australia.

higher-frequency oscillations by the matrix acts to filter out the dominant incident wave forcing frequencies. The presence of a spectral peak in groundwater fluctuation energy at a lower-frequency band has been shown to be as a result of either forcing from input oceanic long waves (which are less damped) or by short waves combining at the beach face in such a way as to appear to the matrix as low-frequency forcing [*Lewandowski and Zeidler*, 1978]. *Waddell* [1980] also observed the presence of a standing wave at the base of the beach with a peak spectral frequency matching that seen in the groundwater.

[6] In more recent times, swash-aquifer interactions have started to receive considerable attention in direct relation to the mobility of beach face sediments. However, in these studies, most of the field data have been limited to observations of pore pressure and surf zone fluctuations only [e.g., *Turner and Nielsen*, 1997; *Horn et al.*, 1998; *Baldock et al.*, 2001; *Butt et al.*, 2001]. The bulk of these studies focused on the pore pressure response to swash overtopping in saturated sediments, i.e., in the seepage face. This study aims to extend this existing knowledge base by focusing on the aquifer response in the vicinity of the water table exit point and further landward.

[7] *Hegge and Masselink* [1991] present a wave-by-wave analysis of the pore pressure response to swash zone forcing at a location predominantly landward of the swash front. They found that the groundwater response to swash zone forcing was dependent on the runup amplitude with three types of interaction identified during a falling tidal stage: (1) A sufficiently small runup amplitude had no effect on the groundwater level, (2) an increase in runup amplitude would temporarily stabilize the (steadily falling) groundwater level, and (3) a runup event that transgressed the mean groundwater level induced a rise in groundwater level.

[8] The location of the water table exit point on the beach face has been recognized as an important factor in the estimation of sediment movement on the beach face [e.g., *Turner*, 1995; *Elfrink and Baldock*, 2002]. *Turner* [1993] developed a model describing the dynamics of the water table exit point in response to tidal forcing using the theory of *Dracos* [1963] which is based only on the force balance on a water parcel at the surface. *Turner* [1993] showed that, at the tidal frequency, the simple theory adequately described the observed water table exit point motion. In this paper, field data on high-frequency exit point motions in response to swash zone forcing illustrate that the *Dracos* [1963] theory is inadequate in this case. A new modified form of the model is presented and is shown provide much better agreement with the data through a parameterization of the effects capillarity which are known to be important at such high frequencies [e.g., *Barry et al.*, 1996; *Li et al.*, 1997b].

[9] Simple 1D vertical diffusion type groundwater flow models have been shown to adequately predict swash-induced pore pressure fluctuations seaward of the exit point within the seepage face [*Turner and Masselink*, 1998; *Baldock et al.*, 2001]. However, as *Baldock et al.* [2001] pointed out, their model was unable to predict the pore pressure fluctuations observed at a point frequently transgressed by the exit point. It is this aspect of swash-aquifer coupling that is the focus of this investigation, with the

aim of clarifying the importance of previously neglected processes.

[10] All of the aforementioned studies focused on the analysis of pore pressure fluctuations with only a few providing direct comparisons with the forcing shoreline position [e.g., *Hegge and Masselink*, 1991]. In this paper, new data on the pore pressure response to swash zone forcing with simultaneous observations of the shoreline (swash front) location and the previously neglected location of the water table exit point are presented and discussed. Additional insights in to swash-aquifer coupling in the vicinity of the water table exit point are discussed.

2. Capillarity Considerations

[11] In the coupling of the swash zone with the aquifer, one of the most influential aquifer characteristics is the presence of moisture above the water table (Figure 1). Because of capillary forces within the interstitial pores, moisture will rise above the water table until either the sand surface is reached and the capillary suction forces can no longer exist (zone A in Figure 1) or the capillary suction forces become balanced by the weight of the water column above the water table (zone B in Figure 1), which ever comes first. Note that the schematization in Figure 1 is an idealization and that the true nature of the moisture/meniscus profile (dash-dotted line) in the field is unknown and is likely to be uneven because of small-scale heterogeneities leading to spatial variations in the pore size distribution.

[12] The presence of moisture above the water table manifests itself as a reduction in the aquifer storage coefficient used in groundwater flow models [e.g., *Duke*, 1972; *Nielsen and Perrochet*, 2000; *Nachabe*, 2002]. According to capillary-free small-amplitude dispersion relation theory [e.g., *Todd*, 1959; *Nielsen et al.*, 1997], the water table wave number is a function of the dimensionless aquifer depth,

$$k \equiv k \left(\frac{n\omega D}{K} \right) = k_r + i k_i \qquad (1)$$

where ω is the oscillation frequency, D is the aquifer thickness, K is the hydraulic conductivity and n is the porosity (storage coefficient).

[13] Thus a reduction in n due to the presence of moisture above the water table results in a reduced wave number which can be interpreted physically as a reduced decay rate (real part, k_r) and an increased speed of propagation (imaginary part, k_i). *Li et al.* [1997b] showed numerically using the capillarity correction term of *Parlange and Brutsaert* [1987], that unless the correction term was used in their model then swash-induced water table waves were unable to penetrate the aquifer over the distances that had been observed in the field [*Waddell*, 1976].

[14] In zone A of Figure 1 where the moisture extends all the way to the sand surface, a disproportionate relationship exists between moisture exchange and pressure fluctuations [e.g., *Gillham*, 1984; *Nielsen et al.*, 1988]. This relationship is illustrated in Figure 2 where for the loss (or gain) of an amount of water of the order less than a grain diameter ($d_{50} \approx 0.2$ mm) the pressure may fluctuate up to the order of a capillary fringe height ($H_\psi \approx 0.5$ m). This phenomenon is
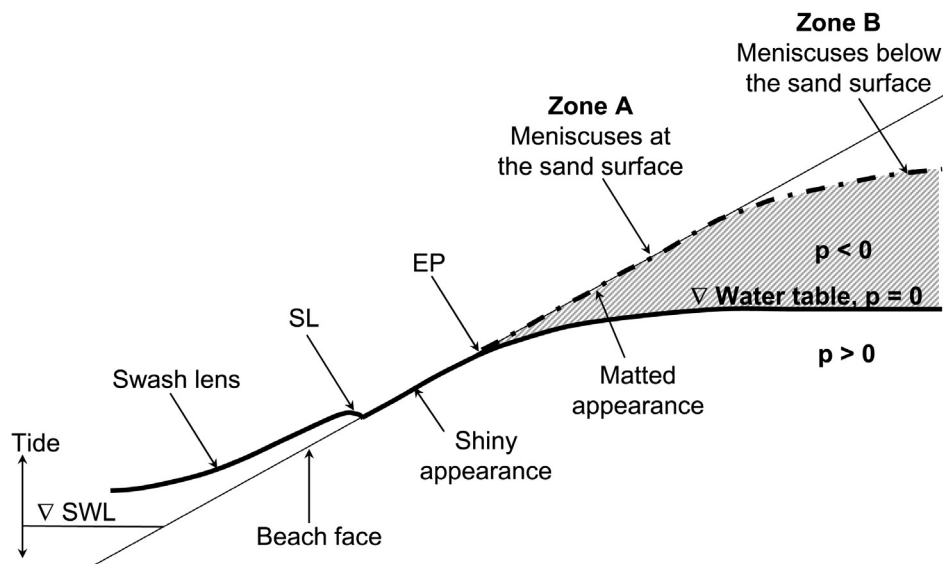
Figure 1. Schematization of the coupling of the swash zone with a sandy beach aquifer. SWL, still water level; SL, shoreline (swash front); EP, water table exit point; p, pore pressure. Bold lines represent the free surface (solid) and idealized meniscus surface (dash-dotted). The shaded region denotes moisture above the water table due to capillary rise.

often referred to as the reverse Wieringermeer effect [e.g., *Gillham*, 1984; *Turner and Nielsen*, 1997]. In order to quantify this phenomenon in terms of a reduction in the aquifer storage coefficient, the dynamic effective porosity concept of *Nielsen and Perrochet* [2000] enables such a parameterization of the effects of capillarity on periodic groundwater flows. The concept relates changes in total moisture to corresponding changes in water table elevation according to the definition,

$$\frac{n_\omega}{n} = \frac{\mathrm{d}h_{tot}}{\mathrm{d}h} \qquad (2)$$

where n_ω is the dynamic effective porosity; n is the drainable porosity; h_{tot} is the equivalent saturated height of total moisture and h is the water table elevation.

[15] Comparing the left and right hand scenarios of Figure 2 for a fine-grained sandy beach, $\mathrm{d}h_{tot} \approx d_{50}$ and $\mathrm{d}h \approx H_\psi$ which leads to,

$$n_\omega = n\frac{\mathrm{d}h_{tot}}{\mathrm{d}h} \approx n\frac{d_{50}}{H_\psi} \qquad (3)$$

Analysis of sediment samples taken from the Belongil Beach field site (described later in section 3.1) by *Robinson et al.* [2005] found the sand to be well sorted with $d_{90}/d_{10} = 1.40$, $d_{50} = 0.28$ mm with a standard deviation $\sigma_\phi = 0.211$ (phi units). Assuming cubic packing of uniform diameter, spherical particles, *Turner and Nielsen* [1997] showed that the height of the capillary fringe can be estimated using,

$$H_\psi = \frac{10\sigma}{\rho g d_{50}} \qquad (4)$$

where $\sigma = 0.073$ N/m is the surface tension of water, $\rho = 1025$ kg/m^3 is the density of seawater and g is the

acceleration due to gravity. With $d_{50} = 0.28$ mm, this yields a value of $H_\psi = 0.26$ m. Returning to the approximation of the dynamic porosity (equation (3)) we find that,

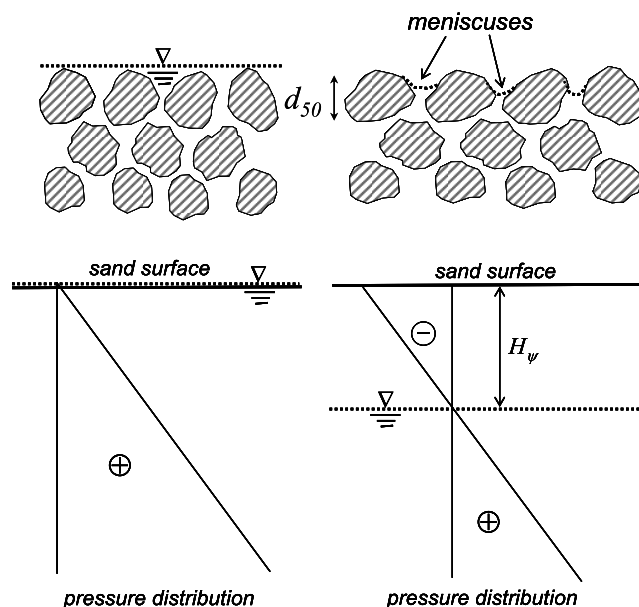$$n_\omega \approx n\frac{d_{50}}{H_\psi} \approx n\frac{0.00028}{0.26} \approx 0.001n \qquad (5)$$

Figure 2. Schematic illustrating the disproportionate relationship between change in total moisture ($dh_{tot} \approx d_{50}$) and corresponding change in pressure head ($dh \approx H_\psi$) when the water table is in close proximity to the sand surface, after *Nielsen et al.* [1988].
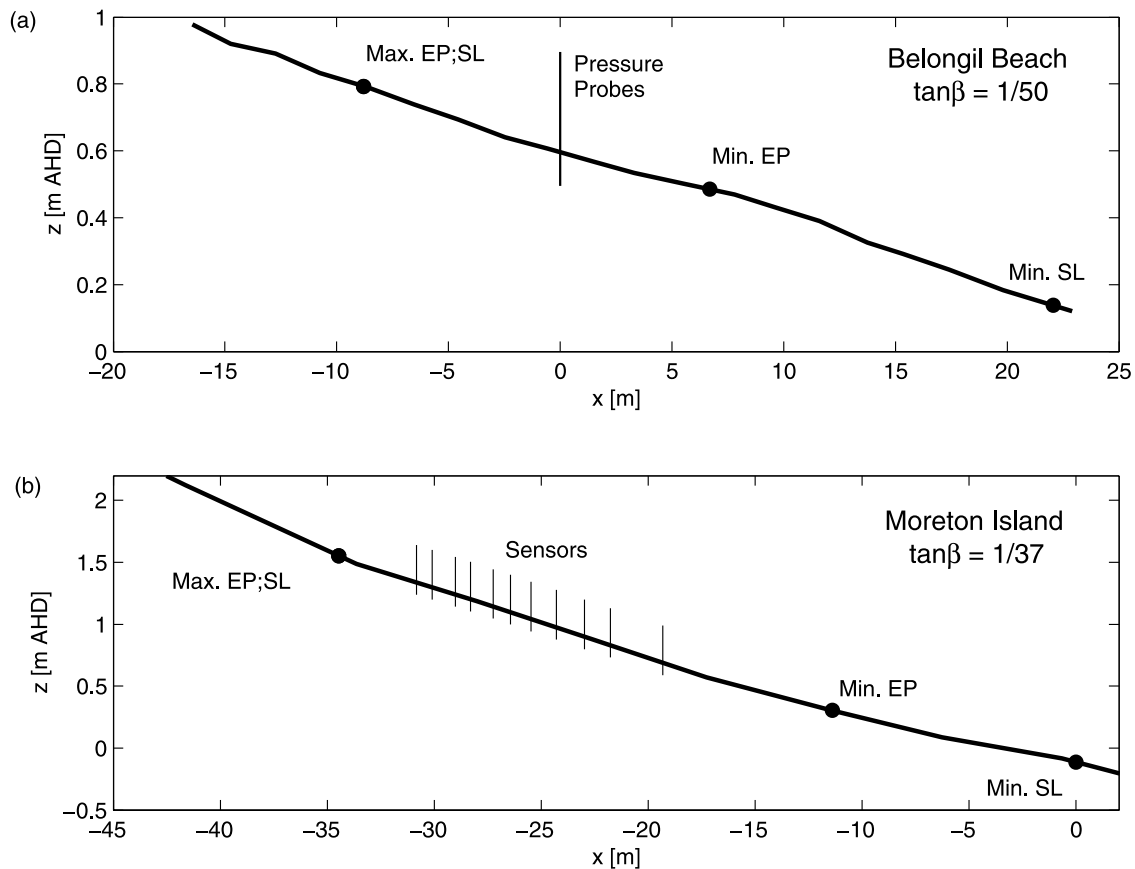
Figure 3. Experimental layouts and maximum and minimum water table exit point (EP) and shoreline (swash front) (SL) locations for the two field sites. (a) Single shore-normal pressure probe location at Belongil Beach. (b) Shore-normal transect of buried sensors at Moreton Island.

i.e., the aquifer storage coefficient in this case is three orders of magnitude less than the classical capillary-free value, n.

3. Field Observations

3.1. Field Sites

[16] Two field experiments were conducted, one at Belongil Beach in northern New South Wales (23 June 2004) and the other on Moreton Island in southeast Queensland (6 December 2004) (see Figure 3). Both sites are fairly typical for the region with median grain sizes of the order 0.2 mm. For the Belongil Beach experiment the beach slope gradient was 0.02, the average deep water significant wave height and peak period were 1.5 m and 12.2 s respectively and the tidal range was 1.3 m. At Moreton Island the beach slope gradient was 0.027, the average deep water significant wave height and peak period were 1.8 m and 7.6 s respectively and the tidal range was 1.1 m.

3.2. Instrumentation and Procedures

[17] The instantaneous shoreline (swash front) location was monitored using a runup wire deployed and maintained 1 to 2 cm above the bed [*Holland et al.*, 1995; *Hughes*, 1995]. The pore pressure was monitored using two different configurations of six cabled pressure transducers capable of measuring both positive and negative pressures. The transducers were logged synchronously with the runup wire, both at 10 Hz.

[18] At Belongil Beach the pore pressure was monitored at a single shore normal location in a vertical array using the pressure probe technique developed by *Baldock and Holmes* [1996]. The set up consists of the transducers, mounted on an external platform, each connected to narrow diameter probes made of 2 mm ID stainless steel hypodermic tubing. The pore pressure is transmitted through the probes via 12, 0.4 mm holes laser drilled near the tip (3 per 90° face). *Baldock and Holmes* [1996] showed that such a system had a natural frequency of about 35 Hz, sufficiently greater than the frequency of natural swash zone motions (about 0.1 Hz) to avoid any issues related to instrument response times. This technique has been used previously in the field to measure swash-induced pore pressure response and vertical gradients very close to the surface of a natural beach [*Horn et al.*, 1998; *Baldock et al.*, 2001].

[19] The Moreton Island experiment focused on capturing the propagation of the swash-induced pore pressure wave and consisted of a shore normal array of the six pressure transducers buried directly into the sand. This inherently avoided any problems resulting from the response time of piezometers or other such groundwater/pore pressure monitoring equipment. The array spanned approximately 10 m cross-shore to capture the propagation and decay of the pressure wave. The elevation of each sensor was nominally set at the "quasi-steady" tidal water table elevation within the beach aquifer.
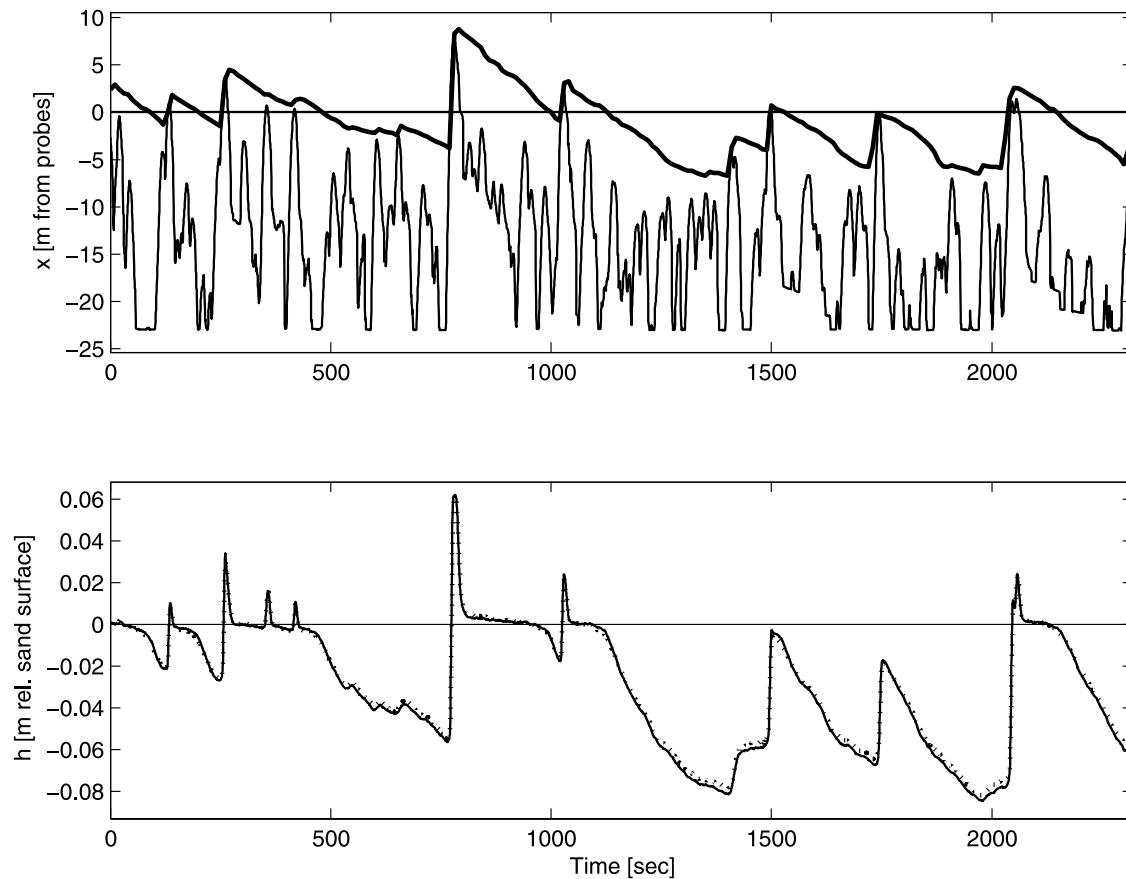
Figure 4. Time series (top) of the shoreline (thin line) and exit point (bold line) locations and (bottom) of the pore pressure response observed at a single shore normal location at elevations of -0.01 m (solid line) and -0.26 m (dotted line) below the sand surface at Belongil Beach.

[20] The water table exit point is easily identifiable on the beach face as the interface between sand with shiny and matt appearances. A shiny, saturated sand surface indicates that the free surface (the water table) is at the sand surface and the matt sand surface immediately landward of the exit point indicates the presence of meniscuses at the sand surface (see zone A in Figure 1). In reality, an exit line exists longshore which is rarely straight because of variations in topography and wave runup in the longshore direction. Hence the exit point as defined here is the intersection of the longshore exit line with the shore-normal instrument transect. The exit point location was monitored by eye with a sampling interval of 15 s using a tape measure laid on the beach face.

4. Results and Discussion

4.1. Pore Pressure Response at a Single Location

[21] Figure 4 shows an example time series of data from Belongil Beach. Figure 4 (top) shows the water table exit point (x_{EP}) and shoreline (x_{SL}) location on the beach face relative to the pressure probe location ($x = 0$). Figure 4 (bottom) shows the corresponding pore pressure response at two different elevations in terms of a pressure head in meters relative to the sand surface ($h = 0$). The head at the two elevations is seen to be quite similar and consider-

ing that a significant body of work on swash-induced pore pressure gradients already exists in the literature [e.g., *Turner and Nielsen*, 1997; *Horn et al.*, 1998; *Turner and Masselink*, 1998; *Baldock et al.*, 2001; *Butt et al.*, 2001], the following discussions will focus on the general trends seen in the pore pressure response rather than on hydraulic gradients.

[22] In confirmation of previous findings [e.g., *Turner and Nielsen*, 1997; *Horn et al.*, 1998; *Turner and Masselink*, 1998; *Baldock et al.*, 2001] the pore pressure is seen to respond instantaneously to an overtopping swash event. Once the shoreline recedes seaward the pore pressure head remains at the sand surface ($h = 0$) indicating that the probes are located within the seepage face, confirmed by the fact that the exit point is landward of the probes. At the instant when the exit point recedes seaward of the probe location the pressure head immediately begins to drop; initially quickly and then at a relatively slower rate. This type of response has been observed previously [*Horn et al.*, 1998; *Baldock et al.*, 2001] but an explanation has not been presented. The present data however permits the following explanation.

[23] Such a situation occurred between 450 and 750 s and can be explained by the distance from the exit point to the moving shoreline (swash front). During the period of initial rapid decline (450–500 s) the shoreline is also rapidly

receding to around 20 m or so seaward of the probes. At around 500 s a series of swash events brings the shoreline to within a few meters of the probes, and this correlates with a reduction in the rate of decline in pressure head at the probes. A decrease in the rate of exit point recession is also apparent. A similar but weaker event occurs between 1200 and 1400 s. *Hegge and Masselink* [1991] made similar observations in that given a sufficient runup amplitude the falling tidal groundwater level was observed to either temporarily stabilize or rise if the mean groundwater level was transgressed.

[24] A further indication of a pore pressure response landward of the shoreline is seen between 1400 and 1800 s. During this time two swash events come within a meter of the probes and the pore pressure is seen to have a strong and instantaneous response. This has been observed previously [*Waddell*, 1976; *Horn et al.*, 1998; *Baldock et al.*, 2001] and is facilitated by the presence of the capillary fringe that provides near-saturation conditions up to the sand surface. As described in section 2, very little moisture exchange occurs (small n_ω) and consequently minimal damping of the pressure pulse occurs, and the speed of propagation remains high, leading to the observed strong and near instantaneous response. The propagation of the pressure pulse into the aquifer is discussed further in section 4.3.

4.2. Water Table Exit Point Dynamics

[25] As discussed in section 4.1 the response of the pore pressure and the water table exit point are clearly connected, with both being strongly influenced by the presence of the capillary fringe. To date, the only attempt to model exit point dynamics at swash frequencies has been undertaken by *Li et al.* [1997b] who coupled the (monochromatic) shallow water equations to a 2D vertical saturated groundwater flow model with the *Green and Ampt* [1911] capillary fringe approximation. They revealed the significant influence of capillarity on exit point motions but noted that the model required validation against data.

[26] In order to further demonstrate the significance of the capillary fringe on water table exit point motion we adopt the simple exit point theory of *Dracos* [1963] which describes the motion of the exit point once it becomes decoupled from the instantaneous shoreline. This enables a direct simulation of the present data by using the observed shoreline to drive the model.

[27] *Dracos* [1963] considered the force balance on a parcel of water at the sand surface but neglected any influence from the subsurface pressure/moisture distribution or the proximity of the shoreline. The force balance yields [*Dracos*, 1963],

$$v_{EP} = \frac{K}{n} \sin^2 \beta \qquad (6)$$

where v_{EP} is the terminal vertical velocity of the exit point postdecoupling, K is the hydraulic conductivity, n is the porosity and β is the beach slope. *Turner* [1993] adopted the *Dracos* [1963] theory and developed a model that accurately predicted the dynamics of the exit point at the semidiurnal tidal frequency (in the absence of waves) where the influence of the capillary fringe is known to be small [e.g., *Barry et al.*, 1996; *Li et al.*, 1997b]. *Turner* [1993]

noted that the model performed poorly when wave heights and hence wave runup activity increased [cf. *Turner*, 1993, Figure 8].

[28] For high-frequency forcing oscillations, capillarity is known to have a significant influence on the water table response [e.g., *Barry et al.*, 1996; *Li et al.*, 1997b; *Turner and Nielsen*, 1997]. Therefore the application of *Dracos*'s [1963] capillary-free theory to the simulation of swash-induced exit point dynamics is to be undertaken with special consideration. In order to illustrate this, *Turner*'s [1993] model was applied without modification using the present shoreline data in place of the tide and is compared to the observed exit point dynamics in Figure 5a. On the basis of sieve analysis data of samples taken from the Belongil Beach site (see section 2) [*Robinson et al.*, 2005], the hydraulic conductivity was estimated using the *Krumbein and Monk* [1942] formulation,

$$K = \frac{kg}{\nu} \text{ where } k = 760D^2 e^{(-1.31\sigma_\phi)} \qquad (7)$$

where ν is the kinematic viscosity of water, k is the permeability in Darcies (1 Darcy = 0.987×10^{-12} m^2), D is the mean grain diameter (assumed here to be equal to d_{50}) and σ_ϕ is the standard deviation in phi units (=0.211, see section 2). The resulting value used in the model was $K = 3.74 \times 10^{-4}$ m/s and the (capillary-free) porosity was set at $n = 0.35$ which is typical for uniform sands ($0.3 < n < 0.4$) [*Bear*, 1972].

[29] The inadequacy of the theory is clearly apparent with the model predicting no visible movement of the water table exit point at this timescale upon the seaward retreat of the shoreline.

[30] In section 2 it was shown that for a situation where saturated moisture conditions exist up to the sand surface, the aquifer storage coefficient can be reduced by three orders of magnitude relative to the capillary-free case (see equation (5)). In the vicinity of the exit point, the capillary fringe will be truncated by the sand surface (see zone A of Figure 1), which will also lead to a further reduction in the storage coefficient [e.g., *Gillham*, 1984]. *Cartwright et al.* [2004b] presented sand column data in which the storage coefficient was further reduced by up to a factor 4 with increasing degrees of truncation. Combining the reduction described by equation (5) along with a conservative factor of 2 reduction for truncation effects leads to the reduced aquifer storage coefficient,

$$n_{red} = \frac{n_\omega}{2} = \frac{0.001n}{2} = \frac{0.001 \times 0.35}{2} = 0.00019 \qquad (8)$$

[31] *Turner*'s [1993] model was modified using the parameterization of capillarity effects described above. When applied to the data, the new modified model provides a much better comparison with the data as shown in Figure 5b. The model closely predicts the general rate of fall of the exit point in most cases.

[32] A detailed sensitivity analysis of the *Dracos* [1963] based exit point model to the hydraulic conductivity and beach slope (with a fixed porosity) has been performed by *Turner* [1993]. However, it is interesting to note that on the basis of using equations (3) and (4) for the reduced porosity
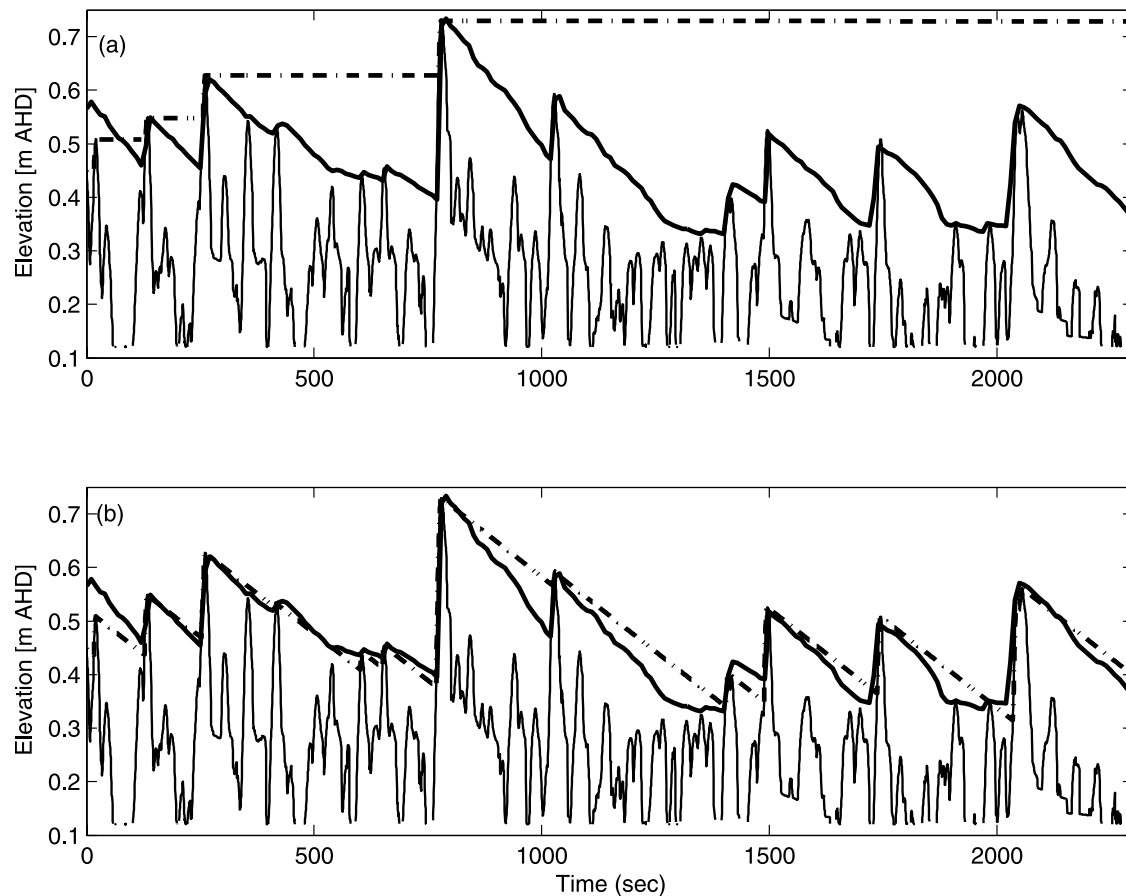
Figure 5. Comparison of observed and simulated water table exit point dynamics from Belongil Beach (a) $n = 0.35$ and (b) $n = n_{red} = 0.00019$. The curves in each panel represent the observed shoreline (thin line) and the observed (bold solid line) and simulated (bold dash-dotted line) water table exit point. Parameters are $K = 3.85 \times 10^{-4}$ m/s and $\tan\beta = 1/50$.

and equation (7) for the hydraulic conductivity, both n_{red} and K are proportional to d_{50}^2. Therefore the ratio K/n_{red} and hence the modified form of the model presented here is independent of d_{50}. The ratio is dependent on the standard deviation in sediment size (σ_ϕ) through the hydraulic conductivity K (see equation (7)) and on the capillary-free porosity (n) through the reduced porosity n_{red} (see equation (8)).

[33] It is prudent to emphasize that the approximations made in relation to the reduced porosity (see equation (3)) are only valid where the capillary fringe extends to the sand surface, a reasonable assumption in the vicinity of the water table exit point on a sloping beach face. Also, as discussed previously in this section, the influence of the capillary fringe on water table fluctuations at the tidal frequency has been shown to be small [e.g., *Barry et al.*, 1996; *Li et al.*, 1997b] and hence a reduction of the porosity as per equation (3) is not required in this situation.

4.3. Pore Pressure Wave Propagation Landward of the Runup Limit

[34] In this section the nature of the pore pressure wave propagation landward of the runup limit of individual swash events is examined. The attenuation of the pore pressure

response to a single swash event is shown in Figure 6. Note that the data is presented as the head fluctuation; that is the local mean (averaged over the time interval plotted) has been removed from each signal. The shoreline just reached the most seaward sensor and the pressure wave is seen to propagate landward through the array over a distance of about 11.5 m before the signal disappears. The time between peaks observed at the most seaward and landward locations was around 50 s.

[35] In contrast however is the observation that the zero upcrossing at each location occurs at virtually the same time ($t \approx 915$ s). This is most likely due to the fact that the swash forcing is made up of many different components each with different frequencies. According to the finite-depth aquifer groundwater wave theories of *Nielsen et al.* [1997] and *Li et al.* [2000], the high-frequency components can have a very fast speed of propagation and hence cause the near instantaneous zero upcrossing at all locations. At the same time however, these high-frequency components have a relatively high decay rate and therefore as time progresses they disappear first leaving the slower moving, lower-frequency components which contribute to the observed time lag between peaks.
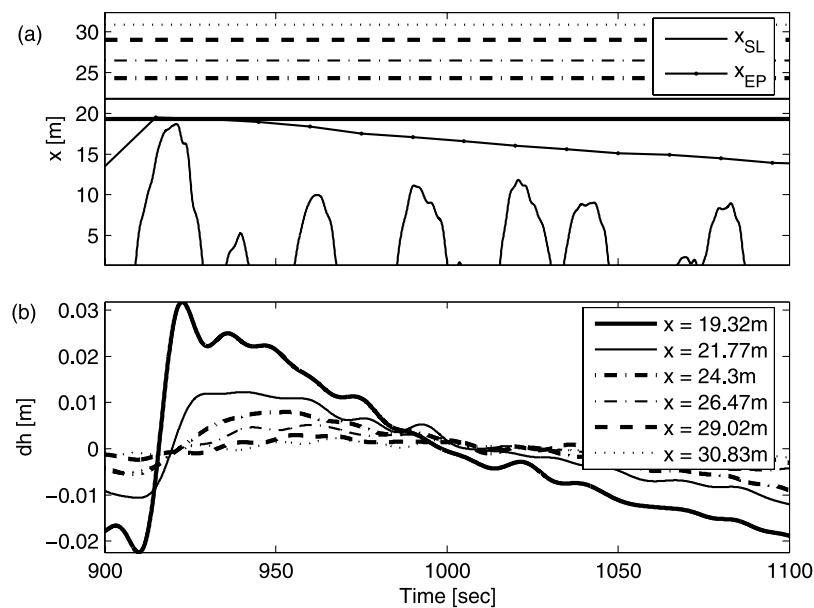
Figure 6. Time series of a single swash-induced pore pressure response at Moreton Island. (a) Shoreline (thin line), exit point (thin solid line with points indicating measurement value) and sensor locations (horizontal lines). (b) Pore pressure head fluctuation (obtained by removing the local mean from each signal) at $x = 19.32$ m (bold solid line); 21.77 m (thin solid line); 24.3 m (bold dash-dotted line); 26.47 m (thin dash-dotted line); 29.02 m (bold dashed line); 30.83 m (thin dotted line). Note that the pore pressure time series correspond to the shore normal locations indicated by the horizontal lines of the same style in Figure 6a.

[36] The pore pressure wave at all locations bears some resemblance to that observed for tidal water table waves [e.g., *Lanyon et al.*, 1982; *Nielsen*, 1990; *Raubenheimer et al.*, 1999] in that they are temporally skewed with a steep rise in pressure followed by a more gradual decline [see also *Hegge and Masselink*, 1991]. For the tidal case this has been explained by the beach matrix being able to "fill more easily than it can drain" [e.g., *Lanyon et al.*, 1982]. More accurately the steep rise is a result of the rising shoreline bringing the forcing closer to the observation point along the sloping boundary, which increases the curvature in the water table and in turn induces a strong inflow into the porous matrix (Figure 7). In contrast, with a falling shoreline, the forcing moves further away from the observation point and the water table curvature becomes relatively flat, leading to a slower outflow (Figure 7).

[37] A different mechanism is responsible for the asymmetry observed for the swash-induced pore pressure wave as the amount of actual "filling and draining" of the beach at this frequency is limited by the presence of moisture above the water table (see section 2). In this case, the rapid rise is attributed to the rapid approach of the instantaneous shoreline during uprush and the slower decline of the pore pressure is due to the water table exit point and instantaneous shoreline decoupling at the start of the backwash phase with the rate of fall of the exit point being much slower than that of the shoreline (see Figure 4).

[38] Five swash events from a single monitoring period were analyzed for decay rates and time lags experienced landward of the runup limit, the results of which are shown in Figure 8. The decay rate has been represented in terms of
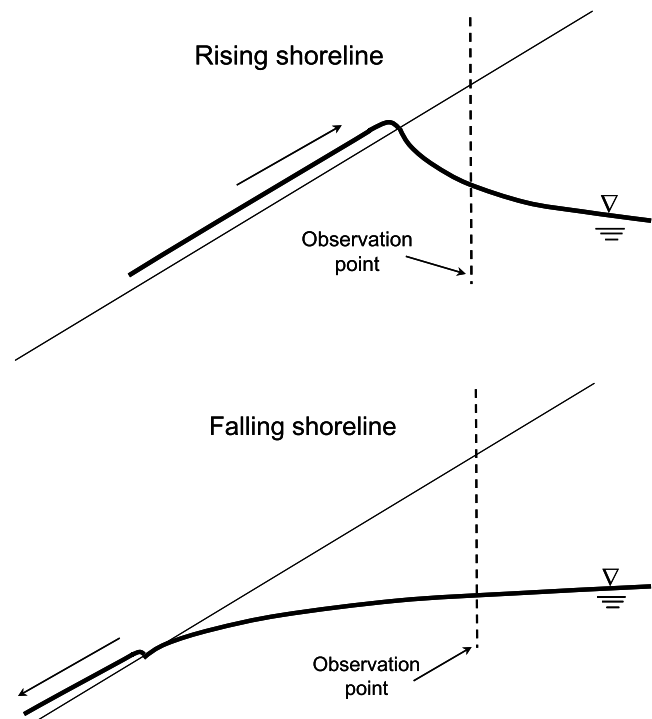

Figure 7. Schematic illustrating the temporal skewing of the observed water table response due to a sloping boundary. (top) During the rising phase, the forcing is brought closer and closer to the observation point, hence the rapid rise in the water table. (bottom) During the falling phase, the forcing moves away from the observation point, hence the relatively slower fall in the water table.
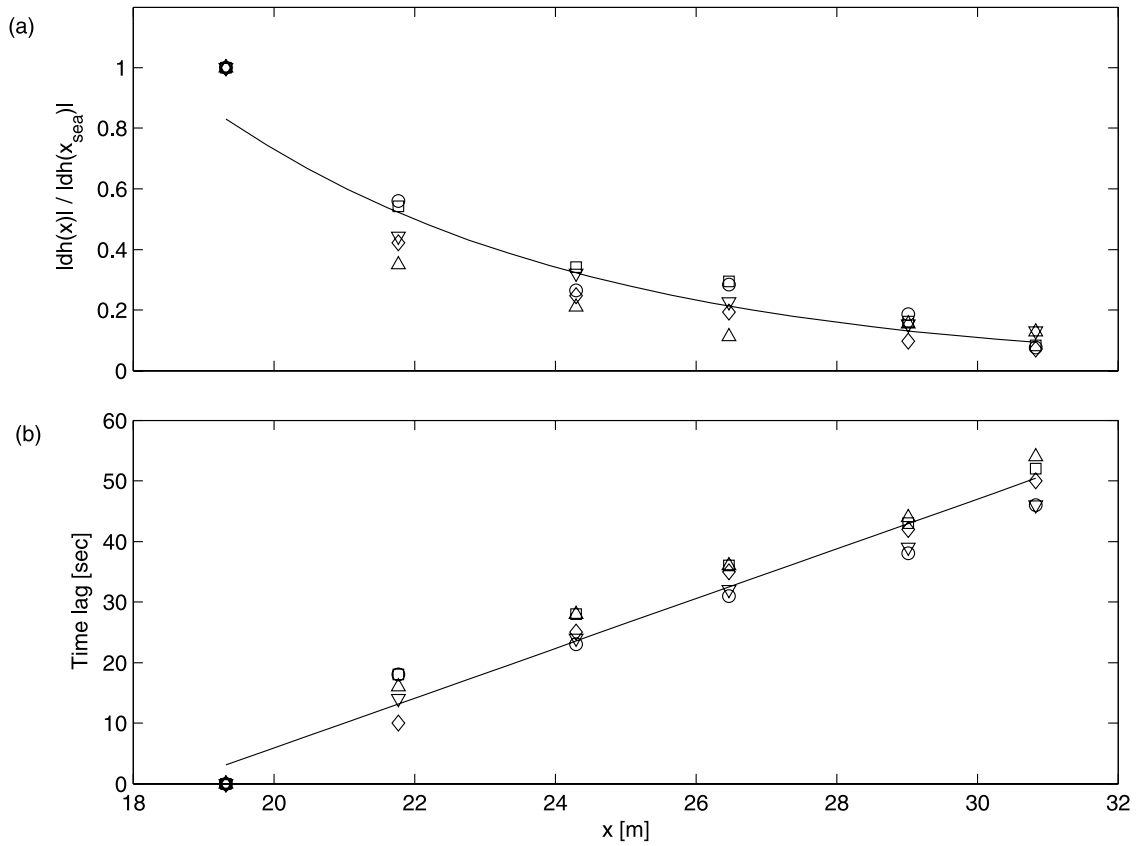
Figure 8. Magnitude and time lag of the pore pressure response landward of the runup limit for 5 swash events (different symbols). (a) Magnitude of the fluctuation range normalized by the magnitude observed at the most seaward sensor ($|dh| = h_{max} - h_{min}$). (b) Time lag relative to the time of the peak at the most seaward sensor. The solid line in each panel shows the exponential and linear trend lines, respectively, fit to all the data.

the magnitude of the pore pressure fluctuation range computed as the difference between the local maximum h_{max} and the head just prior to the event h_{min}, i.e.,

$$|dh(x)| = h_{max} - h_{min} \qquad (9)$$

[39] The results presented have been normalized against the fluctuation observed at the most seaward sensor. An exponential decay rate in each of events is clearly apparent. Curve fitting of the form,

$$|dh(x)| = e^{-kx} \qquad (10)$$

yielded decay rates k in the range of 0.17 to 0.22 m^{-1} with a mean value of 0.19 m^{-1}. The exponential curve fit to all the data shown in Figure 8a has an R^2 value of 0.899.

[40] The time lag was computed as the time between the peak of the most seaward sensor and that observed locally, i.e.,

$$\tau_{lag}(x) = t_{peak}(x) - t_{peak}(x_{sea}) \qquad (11)$$

[41] Each of the events exhibits a linearly increasing time lag and curve fitting of the form,

$$\tau_{lag}(x) = mx \qquad (12)$$

with lag rates m in the range of 3.7 to 4.4 s/m and a mean value of 4.1 s/m. The linear curve fit to all the data shown in Figure 8b has an R^2 value of 0.966.

[42] Although a significant amount of literature is available on the dispersion of water table waves [cf. *Nielsen*, 1990; *Barry et al.*, 1996; *Nielsen et al.*, 1997; *Li et al.*, 2000], all of these theories have been based on simple harmonic forcing where the oscillation frequency is clearly defined. The analysis presented above is on the propagation of the pore pressure wave ahead of single swash events and therefore the choice of frequency enabling a comparison with these theories is not so straight forward. In fact, the pressure waves may be better investigated as the response to a shock wave. This however, is left for future investigations.

[43] The observed trends of an exponential decay rate and linear increase in time lag is the same as observed for tidally induced water table waves [e.g., *Nielsen*, 1990], but have not previously been reported for swash induced events. It is also noted that the decay rates and time lags presented here will vary with tidal stage, beach slope and hydraulic characteristics of the sediment. The variation with tidal stage results from the strong dependence of the dynamic effective porosity (n_ω) on saturation conditions at the surface which are in turn controlled by the tidal stage.

4.4. Shore-Normal Energy Distribution

[44] In order to further investigate the transfer of energy from the swash zone forcing to the pore pressure response, spectral analysis was conducted on each of the measured signals with the intention of determining the peak frequen-
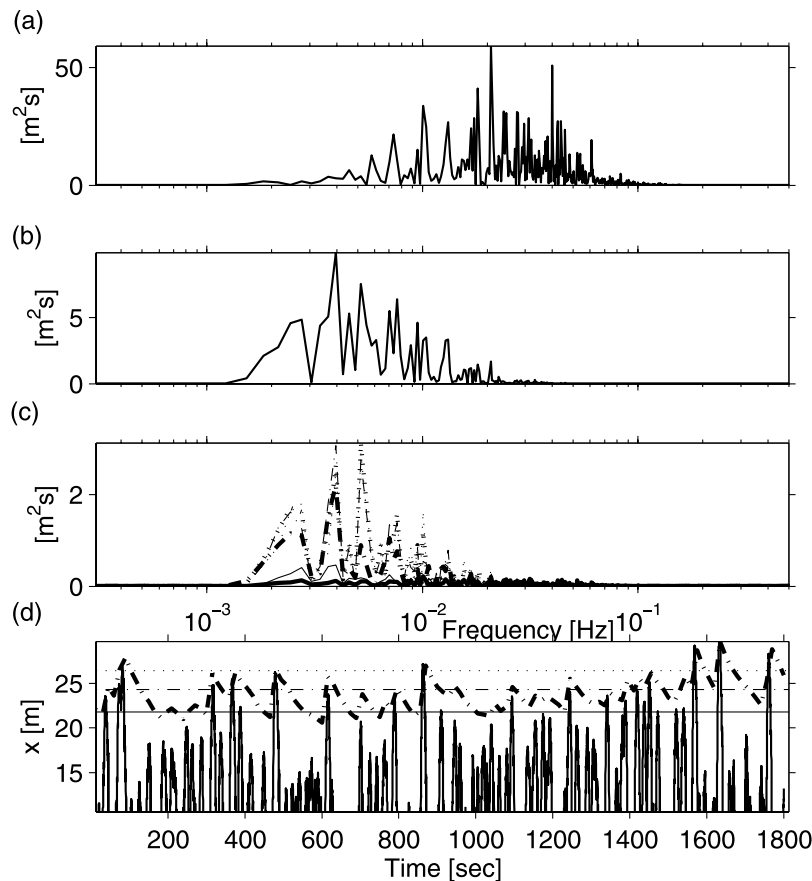
Figure 9. Raw power spectra of (a) the shoreline, (b) exit point and (c) pore pressure respectively. In Figure 9c, the different pore pressure spectra are from the following shore-normal locations: $x = 21.77$ m (bold solid line); 22.97 m (thin solid line); 24.3 m (bold dashed line); 25.47 m (thin dashed line); 26.44 m (bold dash-dotted line); 27.24 m (thin dash-dotted line). (d) Corresponding shoreline and exit point time series illustrating the transgression of wave runup events across the monitoring array. Note that the horizontal lines in Figure 9d denote the sensor locations corresponding to the bold line spectra in Figure 9c.

cies and their relative magnitudes for a single data segment. Although the spectra presented herein are of the raw spectra, corresponding to a large range in confidence intervals (0.3 S(f) and 40 S(f) for the lower and upper 95% confidence limits respectively), it is noted that the spectra are considered here to be representative of the single data segment only and are not representative of a finite sample of an infinite stationary function of time.

[45] Figures 9a–9c show the raw power spectra for the shoreline, exit point and pore pressure respectively, illustrating the preferential filtering of the higher-frequency energy in the shoreline forcing by the beach matrix. Note also that the exit point and pore pressure exhibit peaks at the same frequencies as previously noted by *Nielsen and Turner* [2000].

[46] It is seen that not all of the pore pressure sensors exhibit a significant low-frequency ($f \approx 0.0025$ Hz) peak in energy with the two sensors seaward of the mean exit point showing little energy at this frequency. This is due to the fact that the saturated sand surface within the seepage acts as a "rigid lid," not allowing the pore pressure to fall below the level of the saturated sand surface.

[47] The four sensors landward of the mean exit point exhibit an increase in the magnitude of the low-frequency ($f \approx 0.0025$ Hz) energy peak with distance from the mean exit point position. This is because when a swash event recedes and the exit point moves seaward of the sensor then the pore pressure head is able to drop below the sand surface and, because of the presence of the capillary fringe, experiences limited damping and hence a larger pressure fluctuation, leading to a larger spectral energy density.

[48] This mechanism is further clarified by inspection of the corresponding time series shown in Figure 10. Figure 10b illustrates a time series from a location within the seepage face and the head is seen to remain at a level corresponding to the saturated sand surface when the shoreline is seaward of the measurement location (see Figure 10a). At the location frequently transgressed by the exit point (Figure 10c) the magnitude of the head fluctuation increases. However, at times where the sensor was under the seepage face (e.g., 1550 to 1700 s) the fluctuation range is limited by the saturated sand surface elevation. At a location that was predominantly landward of the exit point (Figure 10d) the range of pressure fluctuation is not limited by a saturated
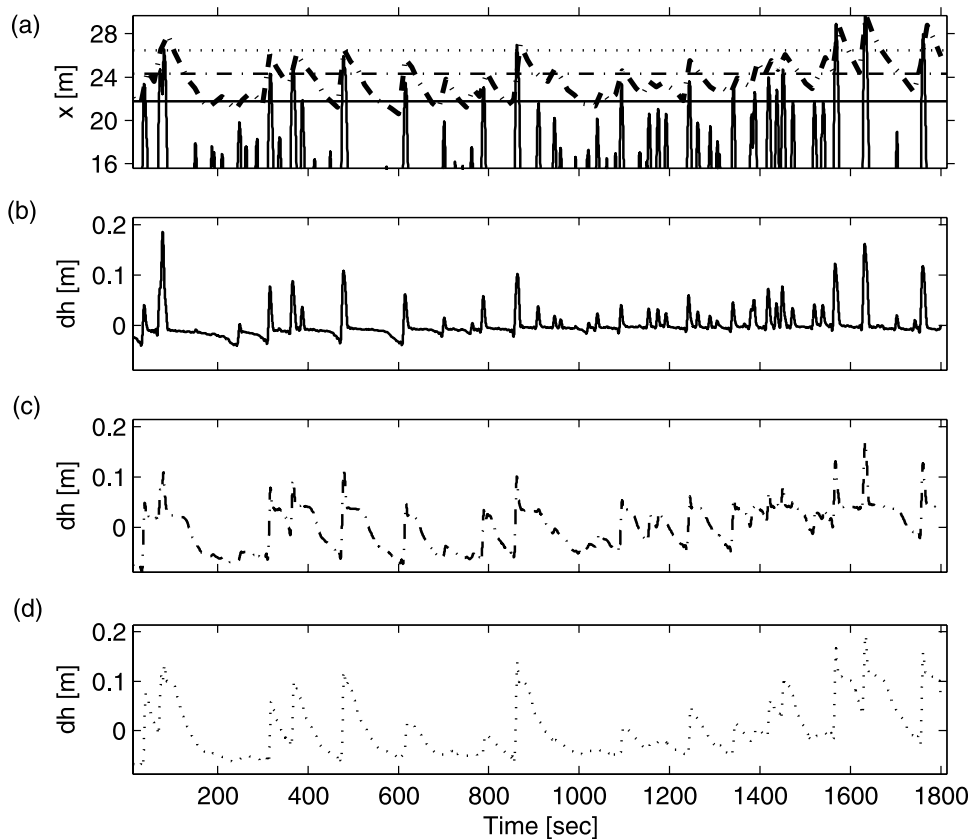
Figure 10. Time series of (a) the shoreline (thin line) and exit point (bold dash-dotted line) and (b−d) the pore pressure response at the shore normal locations $x = 21.8$ m, 24.3 m and 26.4 m respectively. Note that the pore pressure time series correspond to the shore normal locations indicated by the horizontal lines of the same style in Figure 10a.

sand surface and is seen to have a relatively larger head fluctuation.

[49] To further confirm the above discussion, Figure 11c shows the shore-normal variation in peak energy for several peak frequencies with Figures 11a and 11b respectively showing the forcing time series and pore pressure frequency spectrum for reference. Note that a different measurement run has been analyzed here using a run during which the mean exit point was near the seaward limit of the sensor array and the maximum runup limit was within the bounds of the sensor array. This enables the clear illustration of the pore pressure response in three distinct zones in the vicinity of the exit point.

[50] In the first region seaward of the mean exit point, there is relatively little energy at any of the peak frequencies because of the "rigid lid" effect of the seepage face. In the second region between the mean exit point and the maximum runup limit, all frequencies exhibit a significant growth in peak energies. Lastly, the sensors landward of the maximum runup limit all exhibit a strong attenuation of the peak energy.

5. Conclusions

[51] Simultaneous measurements of the shoreline location and corresponding responses of the pore pressure and water table exit point have been presented, revealing new insights into the coupling of the swash zone with sandy beach aquifers. Measurements were taken from both within the seepage face and landward of the exit point.

[52] For the case where the exit point is receding seaward of the measurement location, the pore pressure initially decreases rapidly, followed by a slower decline at a constant rate. The present data indicates that the rate of decrease is directly related to the distance between the shoreline and the exit point; the greater the distance the faster the rate of decline. Future modeling of swash-aquifer interactions in the vicinity and landward of the exit point should therefore include the horizontal shore-normal dimension and not be limited to simplified 1D vertical applications [e.g., *Turner and Masselink*, 1998; *Baldock et al.*, 2001].

[53] A theory describing the motion of the exit point [*Dracos*, 1963; *Turner*, 1993] has been shown to be inadequate in describing the present high-frequency data because of its neglect of subsurface pressure. A new modified version of the *Dracos* [1963] model has been shown to adequately reproduce the general rate of fall of the exit point through a parameterization of the effects of capillarity into the aquifer storage coefficient. The modified model provides a simple means to obtain a sufficiently accurate estimate of the exit point location to determine whether individual swash events transgress the exit line.
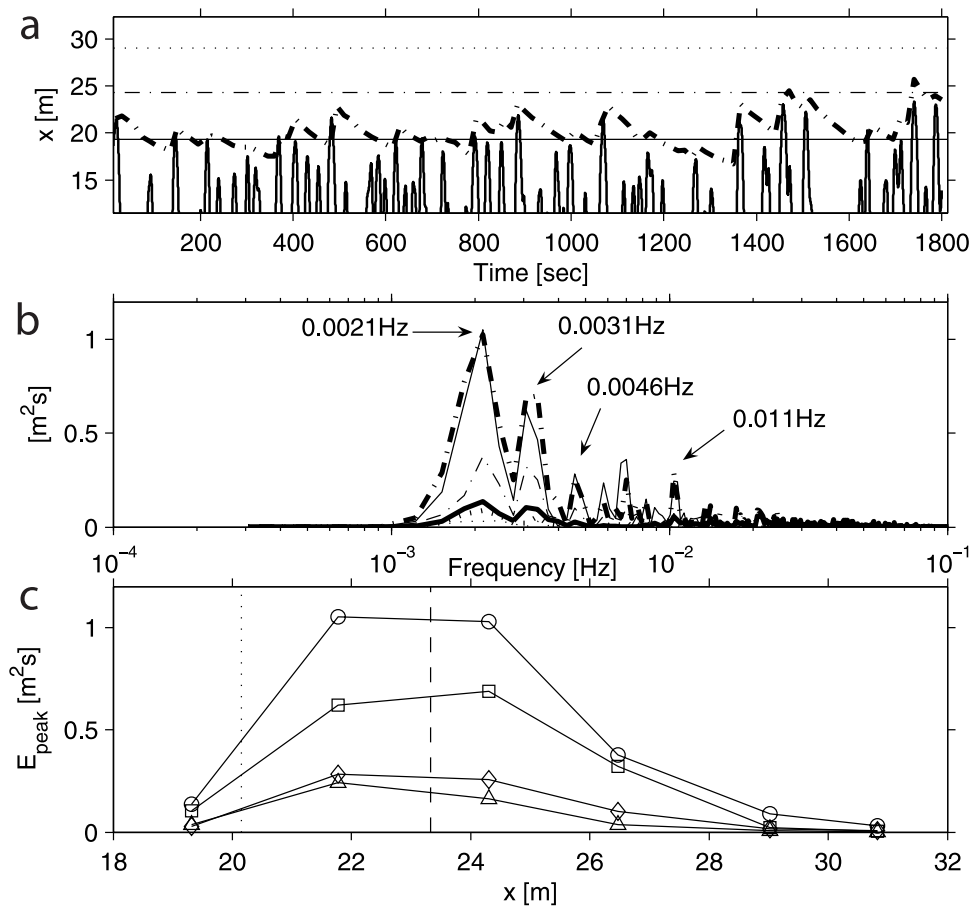
Figure 11. (a) Time series of observed exit point and shoreline location relative to the instrument array (horizontal lines). (b) Raw pore pressure spectra. (c) Shore-normal peak energy profiles corresponding to the peak frequencies shown in Figure 11a: 0.0021 Hz (circles), 0.0031 Hz (squares), 0.0046 Hz (diamonds) and 0.011 Hz (triangles). The vertical lines in Figure 11c are the mean exit point (dotted line) and maximum shoreline (dash-dotted line) positions.

Such predictions are necessary for improved modeling of any influence of infiltration and exfiltration on swash zone sediment transport.

[54] Observations of the pore pressure response landward of the runup limit of individual swash events reveals that the magnitude of the swash induced pressure wave decays exponentially during shoreward propagation into the beach aquifer and the propagation speed is observed to be constant. The shore-normal energy distribution is seen to be strongly dependent on position relative to the water table exit point. Seaward of the exit point peak energies are relatively small because of the saturated sand surface in the seepage face acting as a ''rigid lid.'' Swash events that transgress the exit point exhibit larger peak energies because of the pore pressure head being able to fall below the sand surface and the presence of the capillary fringe which reduces the attenuation of the pressure wave. Further landward a rapid attenuation of peak energies is observed. The magnitude of the fluctuations at any point is dependent on the thickness of the capillary fringe and therefore will vary with beach slope and sediment characteristics in addition to the relative position of the exit line and the magnitude of the shoreline forcing.

References

Baird, A. J., and D. P. Horn (1996), Monitoring and modelling groundwater behaviour in sandy beaches, *J. Coastal Res.*, *12*(3), 630–640.

Baird, A. J., T. Mason, and D. P. Horn (1998), Validation of a Boussinesq model of beach groundwater behaviour, *Mar. Geol.*, *148*(1), 55–69.

Baldock, T. E., and P. Holmes (1996), Pressure gradients within sediment beds, paper presented at 25th International Conference on Coastal Engineering, Am. Soc. of Civ. Eng., Orlando, Fla.

Baldock, T. E., A. J. Baird, D. P. Horn, and T. Mason (2001), Measurements and modeling of swash-induced pressure gradients in the surface layers of a sand beach, *J. Geophys. Res.*, *106*(C2), 2653–2666.

Barry, D. A., S. J. Barry. and J.-Y. Parlange (1996), Capillarity correction to periodic solutions of the shallow flow approximation, in *Mixing in Estuaries and Coastal Seas, Coastal and Estuarine Stud.*, vol. 50, edited by C. B. Pattiaratchi, pp. 496–510, AGU, Washington, D. C.

Bear, J. (1972), *Dynamics of Fluids in Porous Media*, 764 pp., Elsevier, New York.

Butt, T., P. Russell, and I. Turner (2001), The influence of swash infiltration-exfiltration on beach face sediment transport: Onshore or offshore?, *Coastal Eng.*, *42*, 35–52.

Cartwright, N., L. Li, and P. Nielsen (2004a), Response of the salt-freshwater interface to a wave induced groundwater pulse: Field observations and modelling, *Adv. Water Resour.*, *27*(3), 297–303.

Cartwright, N., P. Nielsen, and L. Li (2004b), Experimental observations of watertable waves in an unconfined aquifer with a sloping boundary, *Adv. Water Resour.*, 27, 991–1004.

Dracos, T. (1963), Ebene nichtstatinare Grundwasserabflusse mit freier Oberflache, *Rep. 57*, Tech. Hochsch., Zurich, Switzerland.

Duke, H. R. (1972), Capillary properties of soils—Influence upon specific yield, *Trans. Am. Soc. Agric. Eng.*, 15, 688–691.

Elfrink, B., and T. E. Baldock (2002), Hydrodynamics and sediment transport in the swash zone: A review and perspectives, *Coastal Eng.*, 45(3), 149–167.

Gillham, R. W. (1984), The capillary fringe and its effect on water-table response, *J. Hydrol.*, 67, 307–324.

Green, W. H., and G. A. Ampt (1911), Studies on soil physics 1. The flow of air and water through soils, *J. Agric. Sci.*, IV(I), 1–24.

Hegge, B. J., and G. Masselink (1991), Ground watertable response to wave runup: An experimental study from Western Australia, *J. Coastal Res.*, 7(3), 623–634.

Holland, K. T., B. Raubenheimer, R. T. Guza, and R. A. Holman (1995), Runup kinematics on a natural beach, *J. Geophys. Res.*, 100(C3), 4985–4993.

Horn, D. P., T. E. Baldock, A. J. Baird, and T. E. Mason (1998), Field measurements of swash induced pore pressures within a sandy beach, paper presented at 26th International Conference on Coastal Engineering, Am. Soc. of Civ. Eng., Copenhagen, Denmark.

Hughes, M. G. (1995), Friction factors for wave uprush, *J. Coastal Res.*, 11(4), 1089–1098.

Jackson, N. L., and K. F. Nordstrom (1997), Effects of time-dependent moisture content of surface sediments on aeolian transport rates across a beach, Wildwood, New Jersey, U. S. A., *Earth Surf. Processes Landforms*, 22, 611–621.

Kang, H.-Y., A. M. Aseervatham, and P. Nielsen (1994), Field measurements of wave runup and the beach watertable, *Res. Rep. CE148*, Dep. of Civ. Eng., Univ. of Queensland, Brisbane, Queensl., Australia.

Krumbein, W. C., and G. D. Monk (1942), Permeability as a function of the size parameters of unconsolidated sand, *Am. Inst. Min. Metall. Eng. Tech. Publ.*, 11.

Lanyon, J. A., I. G. Eliot, and D. J. Clarke (1982), Groundwater-level variation during semidiurnal Spring Tidal Cycles on a Sandy Beach, *Aust. J. Mar. Freshw. Res.*, 33, 377–400.

Lewandowski, A., and R. B. Zeidler (1978), Beach ground-water oscillations, paper presented at 16th International Conference on Coastal Engineering, Am. Soc. of Civ. Eng., Hamburg, Germany.

Li, L., and D. A. Barry (2000), Wave-induced beach groundwater flow, *Adv. Water Resour.*, 23, 325–337.

Li, L., D. A. Barry, and C. B. Pattiaratchi (1997a), Numerical modelling of tide-induced beach water table fluctuations, *Coastal Eng.*, 30, 105–123.

Li, L., D. A. Barry, J.-Y. Parlange, and C. B. Pattiaratchi (1997b), Beach water table fluctuations due to wave run-up: Capillarity effects, *Water Resour. Res.*, 33(5), 935–945.

Li, L., D. A. Barry, F. Stagnitti, and J.-Y. Parlange (1999), Submarine groundwater discharge and associated chemical input to a coastal sea, *Water Resour. Res.*, 35, 3253–3259.

Li, L., D. A. Barry, F. Stagnitti, and J.-Y. Parlange (2000), Groundwater waves in a coastal aquifer: A new governing equation including vertical effects and capillarity, *Water Resour. Res.*, 36(2), 411–420.

Longuet-Higgins, M. S. (1983), Wave set-up, percolation and undertow in the surf zone, *Proc. R. Soc. Lond., Ser. A*, 390, 283–291.

McArdle, S. B., and A. McLachlan (1991), Dynamics of the swash zone and effluent line on sandy beaches, *Mar. Ecol. Prog. Ser.*, 76, 91–99.

Moore, W. S. (1999), The subterranean estuary: A reaction zone of ground water and sea water, *Mar. Chem.*, 65, 111–125.

Nachabe, M. H. (2002), Analytical expressions for transient specific yield and shallow water table drainage, *Water Resour. Res.*, 38(10), 1193, doi:10.1029/2001WR001071.

Nielsen, P. (1990), Tidal dynamics of the water table in beaches, *Water Resour. Res.*, 26(9), 2127–2134.

Nielsen, P. (1999), Groundwater dynamics and salinity in coastal barriers, *J. Coastal Res.*, 15(3), 732–740.

Nielsen, P., and P. Perrochet (2000), Watertable dynamics under capillary fringes: Experiments and modelling, *Adv. Water Resour.*, 23(1), 503–515. (Errata, *Adv. Water Resour.*, 23, 907–908, 2000.)

Nielsen, P., and I. Turner (2000), Groundwater waves and water exchange in beaches, paper presented at 27th International Conference on Coastal Engineering, Am. Soc. of Civ. Eng., Sydney, N. S. W., Australia.

Nielsen, P., G. A. Davis, J. M. Winterbourne, and G. Elias (1988), Wave setup and the water table in sandy beaches, *Tech. Memo., 88/1*, NSW Off. of Public Works, Sydney, N. S. W., Australia.

Nielsen, P., A. M. Aseervatham, J. D. Fenton, and P. Perrochet (1997), Groundwater waves in aquifers of intermediate depths, *Adv. Water Resour.*, 20(1), 37–43.

Parlange, J.-Y., and W. Brutsaert (1987), A capillarity correction for free surface flow of groundwater, *Water Resour. Res.*, 23(5), 805–808.

Raubenheimer, B., R. T. Guza, and S. Elgar (1999), Tidal water table fluctuations in a sandy ocean beach, *Water Resour. Res.*, 35(8), 2313–2320.

Robinson, C., T. E. Baldock, and D. P. Horn (2005), Measurement of groundwater and swash interactions on a sandy beach, paper presented at 5th International Conference on Coastal Dynamics, Lab. D'Eng. Mar., Univ. Politec. de Catalunya, Int. Cent. for Coastal Resour. Res., Barcelona, Spain.

Todd, D. K. (1959), *Ground Water Hydrology*, 336 pp., John Wiley, Hoboken, N. J.

Turner, I. (1993), Water table outcropping on macro-tidal beaches: A simulation model, *Mar. Geol.*, 115, 227–238.

Turner, I. (1995), Simulating the influence of groundwater seepage on sediment transported by the sweep of the swash zone across macro-tidal beaches, *Mar. Geol.*, 125, 153–174.

Turner, I., and G. Masselink (1998), Swash infiltration-exfiltration and sediment transport, *J. Geophys. Res.*, 103(C13), 30,813–30,824.

Turner, I., and P. Nielsen (1997), Rapid water table fluctuations within the beach face: Implications for swash zone sediment mobility?, *Coastal Eng.*, 32, 45–59.

Turner, I., B. P. Coates, and R. I. Acworth (1997), Tides, waves and the super-elevation of groundwater at the coast, *J. Coastal Res.*, 13(1), 46–60.

Waddell, E. (1976), Swash-groundwater-beach profile interactions, in *Beach and Nearshore Sedimentation*, edited by R. A. Davis and R. L. Ethington, pp. 115–125, Soc. of Econ. Paleontol. and Mineral., Tulsa, Okla.

Waddell, E. (1980), Wave forcing of beach groundwater, paper presented at 17th International Conference on Coastal Engineering, Am. Soc. of Civ. Eng., Sydney, N. S. W., Australia.

T. E. Baldock and P. Nielsen, Division of Civil Engineering, University of Queensland, Brisbane, QLD 4072, Australia.

N. Cartwright and L. Tao, School of Engineering, Griffith University, Gold Coast, QLD 9726, Australia. (n.cartwright@griffith.edu.au)

D.-S. Jeng, School of Civil Engineering, University of Sydney, Sydney, NSW 2006, Australia.